

Sarcomere strain and heterogeneity correlate with injury to frog skeletal muscle fiber bundles

Tina J. Patel,¹ Ronnie Das,¹ Jan Fridén,² Gordon J. Lutz,³ and Richard L. Lieber¹

¹Departments of Orthopaedic Surgery and Bioengineering, Biomedical Sciences Graduate Group, University of California and Veterans Affairs Medical Centers, San Diego, California 92161; ²Department of Hand Surgery, Sahlgrenska University Hospital, S-413 45 Göteborg, Sweden; and ³Department of Pharmacology and Physiology, Drexel University College of Medicine, Philadelphia, Pennsylvania 19129

Submitted 13 May 2003; accepted in final form 16 June 2004

Patel, Tina J., Ronnie Das, Jan Fridén, Gordon J. Lutz, and Richard L. Lieber. Sarcomere strain and heterogeneity correlate with injury to frog skeletal muscle fiber bundles. *J Appl Physiol* 97: 1803–1813, 2004. First published June 18, 2004; 10.1152/jappphysiol.00505.2003.—Sarcomere length and first-order diffraction line width were measured by laser diffraction during elongation of activated frog tibialis anterior muscle fiber bundles (i.e., eccentric contraction) at nominal fiber strains of 10, 25, or 35% ($n = 18$) for 10 successive contractions. Tetanic tension, measured just before each eccentric contraction, differed significantly among strain groups and changed dramatically during the 10-contraction treatment ($P < 0.01$). Average maximum tetanic tension for the three groups measured before any treatment was 203.7 ± 6.8 kN/m², but after the 10-eccentric contraction sequence decreased to 180.3 ± 3.8 , 125.1 ± 7.8 , and 78.3 ± 5.1 kN/m² for the 10, 25, and 35% strain groups, respectively ($P < 0.0001$). Addition of 10 mM caffeine to the bathing medium decreased the loss of tetanic tension in the 10% strain group but had only a minimal effect on either the 25 or 35% strain groups. Diffraction pattern line width, a measure of sarcomere length heterogeneity, increased significantly with muscle activation and then continued to increase with successive stretches of the activated muscle. Line width increase after each stretch was significantly correlated with the lower yield tension of the successive contractile record. These data demonstrate a direct association and, perhaps, a causal relationship between sarcomere strain and fiber bundle injury. They also demonstrate that muscle injury is accompanied by a progressive increase in sarcomere length heterogeneity, yielding lower yield tension as injury progresses.

mechanics; eccentric contraction; cytoskeleton; laser diffraction

FORCED LENGTHENING OF ACTIVATED skeletal muscle [i.e., eccentric contraction (EC)] results in high-tissue loading and is associated with muscle injury. Despite the common occurrence of ECs, the relationship between eccentric force and lengthening velocity is not easily explained based on classic steady-state cross-bridge theories (22, 52), possibly because force achieved during muscle lengthening is not a simple reflection of rates of attachment and detachment of cross bridges. This may not be surprising because the cross-bridge theory was developed primarily to explain the relationship between energetics and force during muscle shortening (24).

Injury resulting from EC has been described at morphological (14, 18), ultrastructural (15, 16), and light-microscopic (36, 49, 64) levels. Whereas muscle deterioration and soreness are associated with injury, the early causative events seem to

be mechanical in nature (7, 37, 45, 69). Presently, there is not consensus in the literature regarding the mechanical factor(s) that causes muscle injury. We believe that this is primarily due to the imprecise measures of strain that have been used for experiments in rabbit tibialis anterior (TA) (37) and rat soleus muscles (69). These investigators have simply assumed that deformation is equally distributed along the muscle-tendon unit and that sarcomere strain and tissue deformation are synonymous. Additionally, it has been shown that changes in tetanic tension (the most commonly used index of “injury”) can be erroneously inferred when tetanic tension optimum is not reestablished after injury is induced (58). This may also provide some of the explanation for discrepancy among studies.

Defining the mechanical basis of EC-induced muscle injury is important as it provides insights into cellular injury mechanisms and may provide novel information regarding the nature of force transmission in skeletal muscle. Strain-based injury mechanisms may implicate such cellular components as strain-activated ion channels (4, 21), whereas stress-based mechanisms may implicate force transmission by cytoskeletal elements or direct stress applied to the cell (25, 40). Unique insights into injury mechanics are afforded by the use of laser diffraction, which measures not only average sarcomere length (L_s), but also L_s variability within the volume (17, 29, 59, 72). Because L_s variability has been used to explain the unique mechanical behavior of muscle during lengthening (22) and muscle adaptation to injury (46, 70), it is of interest to measure these parameters directly during mechanically induced injury. Therefore, the purpose of this study was to define the relationship between L_s , heterogeneity, and muscle’s mechanical response to ECs.

MATERIALS AND METHODS

Muscle preparation. Experiments were performed on fiber bundles ($n = 33$ muscles) or single fibers ($n = 15$) obtained from the medial head of the TA muscle of adult *Rana pipiens* (nominal snout-vent length = 3 cm), which is composed of only the two fastest amphibian muscle fiber types, type 1 and type 2 (43). All frogs were housed in water-filled tanks with dry surfaces at room temperature and were fed live crickets. Small bundles (~60 fibers) or single fibers were dissected from the medial head of the TA muscle while the muscle was immersed in Ringer solution consisting of (in mM) 115 NaCl, 2.5 KCl, 1.8 CaCl₂, 1.0 MgSO₄, and 3.0 phosphate buffer, and 10 mg/l curare adjusted to pH = 7.10 at 25°C. Animal care adhered to the *NIH Guide for the Care and Use of Laboratory Animals* and was approved

Address for reprint requests and other correspondence: R. L. Lieber, Depts of Orthopaedics & Bioengineering (9151), UC San Diego School of Medicine and VA Medical Center, 3350 La Jolla Village Dr., San Diego, CA 92161.

The costs of publication of this article were defrayed in part by the payment of page charges. The article must therefore be hereby marked “advertisement” in accordance with 18 U.S.C. Section 1734 solely to indicate this fact.

by the University of California-San Diego and Veterans Affairs Committees on the Use of Animal Subjects in Research.

Experimental apparatus. For fiber bundles, after dissection, the specimen was transferred to a custom muscle chamber filled with Ringer solution ($\sim 20^\circ\text{C}$). With the use of 8–0 black-braided silk (Deknatel, Fall River, MA), the origin was secured to a rigid, fixed end, and the insertion site was tied to the lever arm of a servomotor (model 300B, Aurora Scientific, Aurora, ON). At both origin and insertion sites, the specimen was tied as closely as possible to the insertion site of the fiber to minimize series compliance. System compliance, including the transducer, was $\sim 5 \mu\text{m/g}$. For single fibers, methods were essentially as previously described in detail (44). Briefly, intact cells were mounted in a chamber containing room-temperature (25°C) Ringer solution between a force transducer (model 405A, Aurora Scientific) and a high-speed length controller (model 318B, Aurora Scientific) by securing the tendons to 125- μm titanium wires with the use of 10–0 silk suture loops. The force transducer and motor were mounted independently on XYZ translation stages to permit precise fiber alignment.

Muscle activation was provided by an electrical stimulator (model S88, Grass Instruments, Quincy, MA) in series with a bipolar power amplifier (model 510, Hewlett-Packard, Cupertino, CA) applied via platinum plate electrodes extending along the length of the bundle. All contractions reported were performed while stimulating at supramaximal levels with a 0.3-ms pulse duration and 100-Hz stimulation frequency. Lever arm movement was induced by using a programmable function generator (model 3314A, Hewlett Packard). The servo system, stimulator, and function generator were all controlled by an acquisition program written in the LabWindows environment (National Instruments, Austin, TX) and data-acquisition board (model 512, Gage, Montreal, Quebec) running on a personal computer (Datal Computers, San Diego, CA).

L_s determination. Whereas numerous previous studies have calculated sarcomere strain during EC, L_s and line width (W) during EC have never been published. Thus L_s was measured during EC by using laser diffraction (41). He-Ne laser light was projected through the fiber(s) from below, and the first-order portion of the diffraction image projected onto a one-dimensional charge-coupled device array camera clocked by a controller (models LC1911/RS1910, EG&G Reticon, Sunnyvale, CA) that was interfaced to the data-acquisition board. Nominal beam diameter was 1.0 mm, but, based on the Gaussian intensity distribution, 66% of the laser intensity was concentrated in the central 0.6 mm. Based on the average fiber length (L_f) of 7.64 mm (see below), $\sim 8\%$ of the sarcomeres within the specimen contributed to the diffraction pattern. The beam was placed as close to the fixed end of the specimen as possible to minimize fiber translation across the laser beam. L_s was calculated based on the distance between the centroids of the first- and zeroth-order diffraction lines, by using the standard grating equation, $n\lambda = L_s \sin\theta$, where n is diffraction order (± 1 in all experiments reported here), λ is laser wavelength (0.632 μm), and θ is diffraction angle relative to the undiffracted zeroth-order beam. L_s heterogeneity was quantified from the W of the first-order peak. W was calculated by using the equations derived by Marikhin and Myasnikova (48) and previously implemented on whole muscle (56) and single cells (17, 29, 57), where:

$$M_0 = \sum_{i=1}^{1,024} A_i$$

$$M_1 = \sum_{i=1}^{1,024} i \cdot A_i$$

and

$$M_2 = \sum_{i=1}^{1,024} i^2 \cdot A_i$$

are the zeroth (M_0), first (M_1), and second (M_2) moments of the diffraction peak, respectively, A_i is the amplitude of the i th photodiode array element, and W is calculated from these moments as:

$$W = 2 \cdot \sqrt{\frac{M_2}{M_0} - \left(\frac{M_1}{M_0}\right)^2}$$

These equations and their application to active and passive muscle were experimentally validated by comparing light microscopic observation of sarcomere populations with the diffraction patterns obtained on whole muscles (56) and single-muscle fibers (10, 29, 57) and are supported by comprehensive theories of light diffraction that explain diffraction peak position, intensity, and W based on the known properties of muscle sarcomeres and fibers (17, 34, 72). Diffraction data were acquired on a 1,024-element array at a rate of 250 kHz (4.096 ms per frame of 1,024-element array) for 1 s, yielding 244 spectra of diffraction data for each contraction.

Before contractile experiments, fiber(s) was checked for diffraction quality. If the resting diffraction pattern from the fiber bundles was poor (i.e., diffraction orders were faint or diffuse or the plus/minus diffraction orders were of dramatically different intensities), the sample was discarded. ECs were initiated at a resting L_s of $\sim 2.4 \mu\text{m}$, which was chosen to permit the specimens to shorten to $\sim 2.2 \mu\text{m}$ during the isometric contraction (IC) phase before the EC (Fig. 1). This ensured that ECs occurred on the descending limb of the length-tension curve, where injury is believed to be more severe, but not at such long lengths that passive tension would confound stress measurements (53, 65).

Fiber-length determination. Rather than attempting to measure fiber bundle length directly (which is prone to error in these fiber bundles due to the staggered fiber insertions onto the tendon), L_f was calculated for each bundle by applying a slow 1-mm-length ramp to the bundle and measuring the accompanying L_s change. The L_s change was divided into the imposed length change to yield serial sarcomere number, which was then multiplied by initial L_s to yield L_f . For each bundle, average L_f calculated from three length ramps was used to determine the length change required to impose a selected nominal strain onto the bundle during experimentation. Average L_f of all bundles tested was $7.64 \pm 0.22 \text{ mm}$ at a nominal L_s of 2.4 μm ($n = 33$). Pilot studies were performed to validate that L_f calculated by using this method represented an accurate measure of actual L_f . L_f measured by using architectural analysis of single fibers dissected from fixed tissue were compared with those measured by using laser diffraction of the fresh tissue before fixation and agreed to within $0.17 \pm 0.19 \text{ mm}$ (mean \pm SD, $n = 20$ independent measurements).

Choice of experimental model. The isolated frog single fiber has historically represented the preparation of choice for high-resolution muscle mechanical studies (12, 13, 20) and for definition of the structural basis for fiber types in frogs (32, 33, 42–44). Unfortunately, pilot experiments ($n = 15$) indicated that the single fiber is much more mechanically fragile when subjected to the active lengthening protocol described below compared with small bundles of fibers. Pilot experiments demonstrated that single fibers subjected to a nominal strain of $\sim 10\%$ generated a stress of $255.2 \pm 11.5 \text{ kN/m}^2$ before treatment, but only $55.4 \pm 8.8 \text{ kN/m}^2$ after the 10-EC sequence ($n = 8$, values not including failed fibers). This was a much more dramatic decrease compared with that observed for fiber bundles at 10% strain, which showed only a very slight decrease (see below). Furthermore, of the 15 single fibers tested, 7 actually ruptured (from contraction 3 to contraction 9) during the eccentric testing protocol. The marked difference between mechanical response of single fibers and bundles was associated specifically with active lengthening, because, after 10

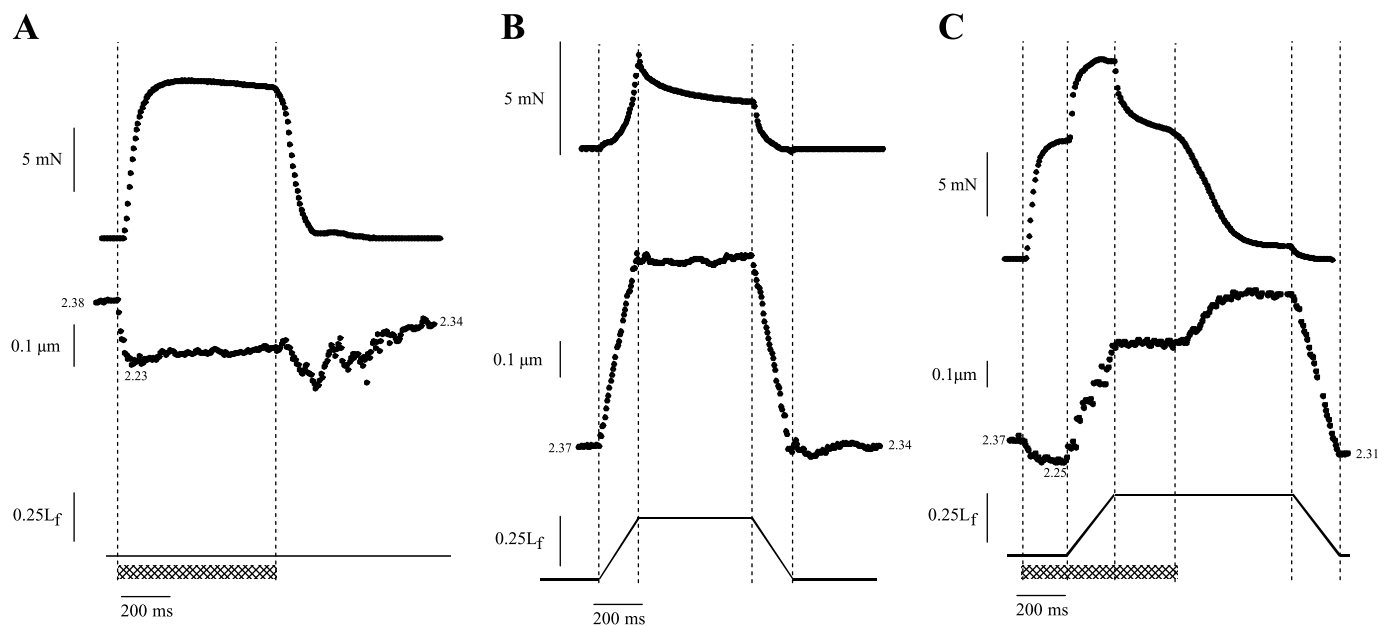


Fig. 1. Muscle force (*top traces*), sarcomere length (*middle traces*), and fiber bundle length (L_f ; *bottom traces*) associated with the contractile experiments performed. These parameters are demonstrated under conditions of isometric contraction (*contraction 1*; A), passive stretch (PS) of 25% strain (*contraction 3*; B), and eccentric contraction (EC) of 25% strain (*contraction 9*; C). Cross-hatched bar (A and C) at bottom indicates the period during which the muscle is electrically stimulated. Vertical lines denote corresponding time periods between force, sarcomere length, and L_f records. Sarcomere length values on traces represent group means across all specimens and thus may not exactly fit the trace shown.

ICs, single fibers showed only a minor force loss, and none ruptured (data not shown), as has been demonstrated in numerous laboratories (12, 19, 26, 35, 44). Determination of the cellular and molecular mechanisms responsible for this provocative difference in mechanical stability between single fibers and fiber bundles is beyond the scope of this investigation. Nonetheless, given that physiological sarcomere strains often exceed 10% (9), we concluded that the single cell was not the appropriate model to use for this investigation and thus performed the majority of this study using small fiber bundles.

Experimental design. Fiber bundles were randomly assigned without replacement into either EC ($n = 18$), passive stretch (PS; $n = 9$), or IC ($n = 6$) treatment groups. In this study, the EC and PS groups were further subdivided into three different nominal fiber strains of 10, 25, and 35% of L_f to understand this mechanical factor's relationship to injury based on the consensus observation that strain velocity has little or no effect on injury magnitude (37, 45, 69). Each experimental treatment consisted of 10 contractions separated by a 3-min interval to minimize muscle fatigue. For bundles subjected only to IC, bundles were held at a resting L_s of $\sim 2.4 \mu\text{m}$ and activated for ~ 600 ms. L_s decreased exponentially to $\sim 2.2 \mu\text{m}$ during stimulation due to series compliance and returned to $\sim 2.3 \mu\text{m}$ after cessation of stimulation (Fig. 1A). Fiber bundles subjected to PS were stretched without activation, to a selected strain, held at the stretched length, and then returned to the original length (Fig. 1B). For the EC groups, muscle were activated isometrically for 200 ms (Fig. 1C) and then lengthened at $2 L_f/\text{s}$, resulting in a dramatic tension rise and L_s increase. Tension increased in two phases, a reflection of the short-range stiffness of skeletal muscle (23), whereas L_s increased linearly. The first phase was a high-stiffness phase and was followed by a "yield" of the muscle to a more compliant phase (see schematic diagram in Fig. 1 of Ref. 60). Muscle length was then held constant for 400 ms during which time tension decayed to a new steady state, whereas L_s remained relatively constant (termed "active hold"). Muscle stimulation was then discontinued, resulting in a force decline, and L_s typically increased as the series compliance recoiled (termed "passive hold"). Finally, muscle fiber bundle length was returned to the initial length, resulting in L_s decrease and reestablishment of resting L_s .

For bundles subjected to EC, L_s and W were measured continuously but analyzed at specific time points: initially, at the end of the IC period, after muscle elongation, at the end of the active hold phase, at the end of the passive hold phase, and after the muscle was returned to its original length. For the IC group, they were measured continuously but analyzed initially, at the end of the IC period, and after cessation of stimulation. For the PS groups, these parameters were measured continuously but analyzed initially, at the end of PS, and after return to rest length. For all groups, force corresponding to each of these time periods was also recorded.

Ten minutes after EC, IC, or PS treatment, post-EC testing was performed on each bundle after experimentally reestablishing optimal length with the use of twitch contractions. This would have the effect of providing a slightly longer optimal length than would be obtained with tetanic contractions (2, 11). Testing consisted of passive stiffness and maximum titanic tension (P_o) measurements every 10 min for 30 min. The three repeated measures were used to assess bundle stability. No change in any properties was measured over this 30-min period, and thus only the initial post-EC results are presented. Finally, after 30 min, the muscle chamber was flushed of its Ringer solution and replaced by a new solution of Ringer containing 10 mM caffeine (Ringer + caffeine). After 1 h of incubation in Ringer + caffeine, P_o was remeasured.

After contractile experiments, bundles were removed from the chamber, weighed, and placed between two layers of porcine gel (15% wt/vol in Ringer solution) for mechanical and cryo-protection. The gel-muscle sandwich was frozen in isopentane cooled by liquid nitrogen (-159°C) and stored at -80°C . Bundle cross-sectional area was calculated from the measured mass and L_f , assuming a muscle density of 1.056 g/cm^3 (50).

SDS-PAGE analysis of myosin heavy chain isoforms. Myosin heavy chain (MHC) isoforms from bundles were separated by SDS-PAGE (31), as previously described (43). Briefly, a $10\text{-}\mu\text{m}$ transverse section was cut from the muscle midbelly and immediately immersed into SDS-PAGE sample buffer. This sample was boiled for 2 min and stored at -80°C before loading onto the gel. Gel components were identical to those used previously for the separation of the rat MHCs

(66). Gels (16×22 cm, 0.75 mm thick) were run at a constant current of 10 mA until voltage rose to 275 V and, thereafter, at constant voltage for 21 h at $4-6^\circ\text{C}$. Silver staining (Bio-Rad, Hercules, CA) was performed according to manufacturer's protocol, except for an additional 40 min of fixation to reduce background staining. Dried gels were optically scanned, and densitometry was performed to quantify the relative proportion of MHC isoforms present in each specimen. Because the bundles were dissected from the medial head, where only two of the four MHCs are present (43), results were presented in terms of the percentage of type 1 and type 2 MHC isoforms present.

Data analysis. For comparison between parameters measured pre- and posttreatment, one-way ANOVA with repeated measures was used. For comparison between strain groups and across contraction number, two-way ANOVA with repeated measures was used. To assess the relationship between fiber strain and muscle injury, P_o decrease was regressed individually on stress and strain and in multiple linear combination by using simple and multiple linear regression. When variables were expressed as percentages, they were arcsine transformed before one-way ANOVA to satisfy the assumption of normality and skew (63). For comparison between measured fiber strain and a particular target strain and comparison of change scores to zero, a one-sampled t -test was used. Level of statistical significance was set to $P < 0.05$.

RESULTS

Peak stress during treatment. Peak stress characteristically reflected the type of treatment imposed on the fiber bundle. For the IC group, peak stress showed no significant change over the 10-contraction treatment paradigm, staying constant at an average level of 222.4 ± 4.2 kN/m² ($P > 0.9$; Fig. 2A, solid symbols). For bundles subjected to EC, peak stress was $\sim 50\%$ greater than that observed during IC (average across strain groups and contractions was 311.5 ± 3.6 kN/m²; Fig. 3A), and two-way ANOVA of stress in bundles subjected to EC demonstrated no significant effect of strain ($P > 0.6$) and a significant effect of contraction number ($P < 0.05$). Specifically, peak EC stress for the first contraction of each strain group was 336.1 ± 9.9 , 349.8 ± 16.3 , and 332.1 ± 12.0 kN/m², all of which were not significantly different from one another ($P > 0.6$), and decreased to 285.9 ± 13.2 , 281.1 ± 26.5 , and 261.9 ± 18.0 kN/m² for the last contraction of the 10, 25, and 35% strain groups, respectively, all of which were not significantly different from one another ($P > 0.8$). Thus, in the EC experimental paradigm, fiber bundles stretched by different amounts resulted in similar stresses throughout the treatment. For bundles subjected to PS, no significant stress change was seen as a function of contraction number for any strain group ($P > 0.9$), but a significant difference between groups was seen ($P < 0.01$, Fig. 2A, open symbols) as expected. Specifically, passive stress was 2.3 ± 0.6 , 25.6 ± 3.5 , and 61.9 ± 16.7 kN/m² for the first stretch, and none of these values changed significantly to 4.2 ± 1.3 , 37.6 ± 11.5 , and 76.2 ± 27.8 kN/m² for the last stretch of the 10, 25, and 35% strain groups, respectively ($P > 0.1$).

Isometric stress before each EC. In contrast to peak stress measured during active stretch, peak isometric stress measured during the 200 ms before active stretch changed significantly during the 10-contraction treatment ($P < 0.001$) and was significantly different among strain levels ($P < 0.01$), as revealed by two-way ANOVA (Fig. 3B). Isometric stress measured before 10% L_f stretch decreased slightly but signifi-

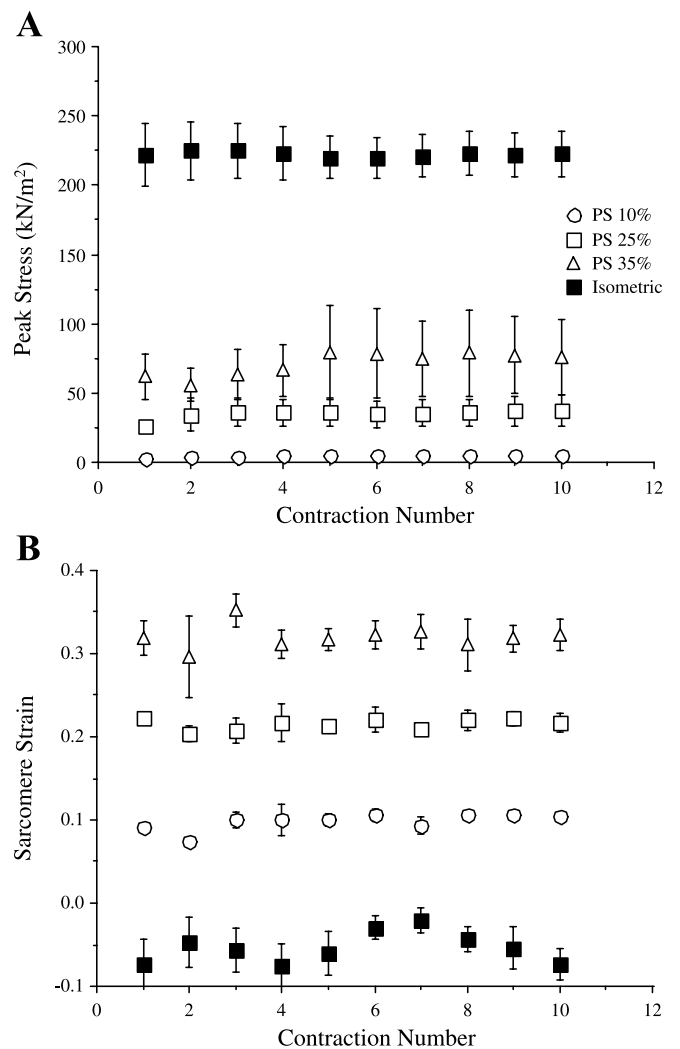


Fig. 2. Time course of peak fiber stress (A) and sarcomere strain (B) associated with PS (\circ , 10% nominal passive strain; \square , 25% nominal passive strain; \triangle , 35% nominal passive strain) or isometric contraction (\blacksquare). Ten of each type of contraction were applied to the fiber at 3-min intervals. Values are means \pm SE.

cantly from an initial value of 207.5 ± 8.3 kN/m² to a final value of 172.8 ± 3.5 kN/m². At the other extreme, isometric stress measured before 35% L_f stretch decreased dramatically from an initial value of 193.7 ± 9.0 kN/m² to a final value of 76.8 ± 8.9 kN/m². Thus, despite the fact that all bundles subjected to EC bore similar stress levels (Fig. 3A), the magnitude of stress that they could generate isometrically just before the eccentric phase of contraction varied significantly between groups and changed significantly over the treatment period.

Changes in P_o . To determine whether the changes in isometric stress measured during the EC bout reflected actual muscle injury rather than a systematic shift in L_o , P_o was remeasured 30 min after the EC bout after L_o was reset by using twitch contractions. For each experimental group, P_o measured after 10 ECs significantly decreased relative to P_o measured before experimental treatment ($P < 0.04$, Fig. 4A) and was significantly different among the three strain groups ($P < 0.0001$; Fig. 4A). Thus, after subjecting fibers to 10% EC, P_o decreased significantly but modestly from 213.8 ± 6.9 to

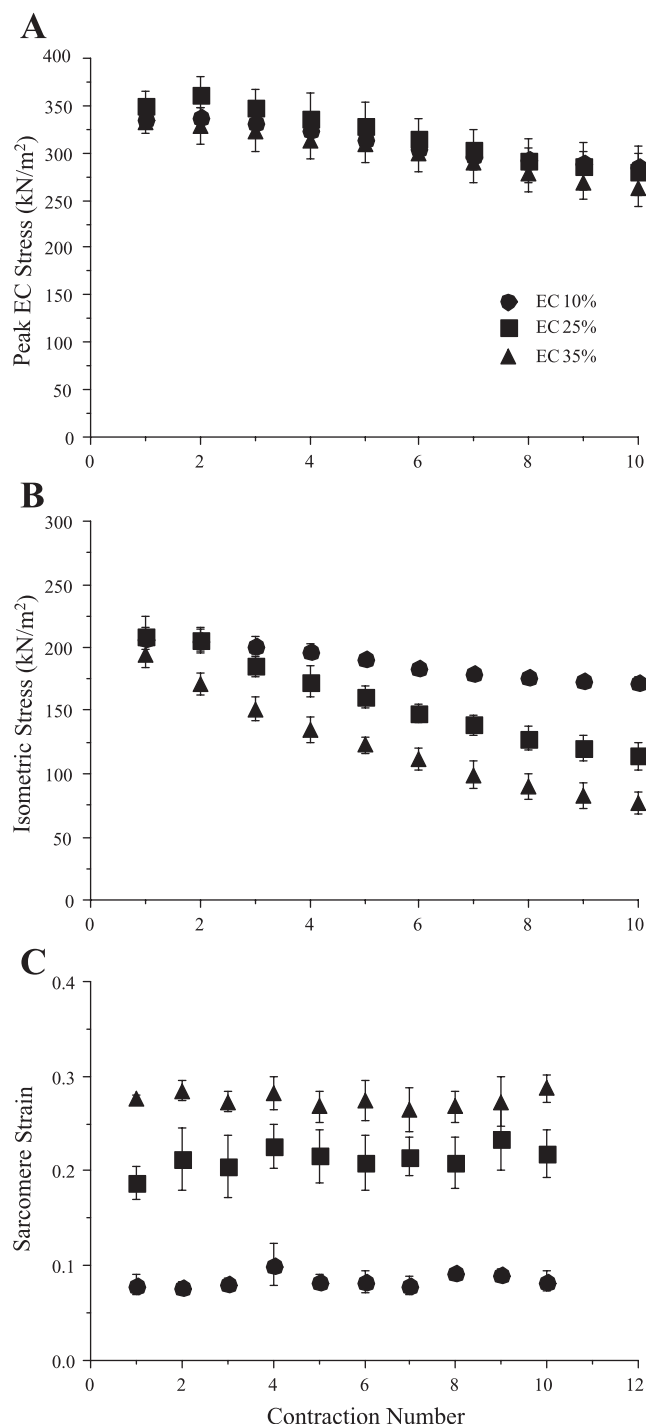


Fig. 3. Time course of peak eccentric muscle fiber stress (A), isometric muscle fiber stress generated immediately before active stretch (B), and sarcomere strain (C) for 10% nominal eccentric strain (●), 25% nominal eccentric strain (■), and 35% nominal eccentric strain (▲). Ten of each type of contraction were applied to the fiber at 3-min intervals. Values shown are means \pm SE.

180.3 ± 3.8 kN/m² or by $\sim 16\%$ ($P < 0.005$). This was in contrast to the tremendous decrease from 255.2 ± 11.5 kN/m² to only 55.4 ± 8.8 kN/m² for single cells subjected to 10% strain. After fiber bundles were subjected to 35% EC, P_o decreased dramatically from 200.9 ± 9.0 to 78.3 ± 5.1 kN/m² or by $\sim 60\%$ ($P < 0.0001$). P_o in bundles subjected to 25% EC

decreased moderately from 216.8 ± 8.1 to 125.1 ± 7.8 kN/m² or by $\sim 40\%$. The percent change in P_o measured before and after the EC bout was nearly identical to the change in peak isometric stress measured from the 1st to 10th EC contraction (16 vs. 17%, 42 vs. 46%, and 62 vs. 60%) for the 10, 25, and 35% nominal strain groups, respectively. In other words, there was no change in P_o measured just before the 10th EC and 30 min after the EC bout following correction for a shift in L_o . This provides strong evidence that the isometric stresses measured during this treatment estimate the functional capacity of the muscle bundle and do not simply result from progressive sarcomere reorganization that could systematically alter L_o or affect force production due to intersarcomere dynamics.

Previous authors demonstrated that some or all of the drop in P_o after EC was reversed by the addition of caffeine (3, 68). To address the extent of excitation-contraction uncoupling in the present experiments, P_o was measured after 1 h in bathing medium consisting of Ringer + caffeine. The 16% decrease in P_o after 10% EC was reversed after the addition of caffeine to a value not significantly different from the initial value of P_o (Fig. 4A, dashed line above solid bars; $P > 0.1$) but signifi-

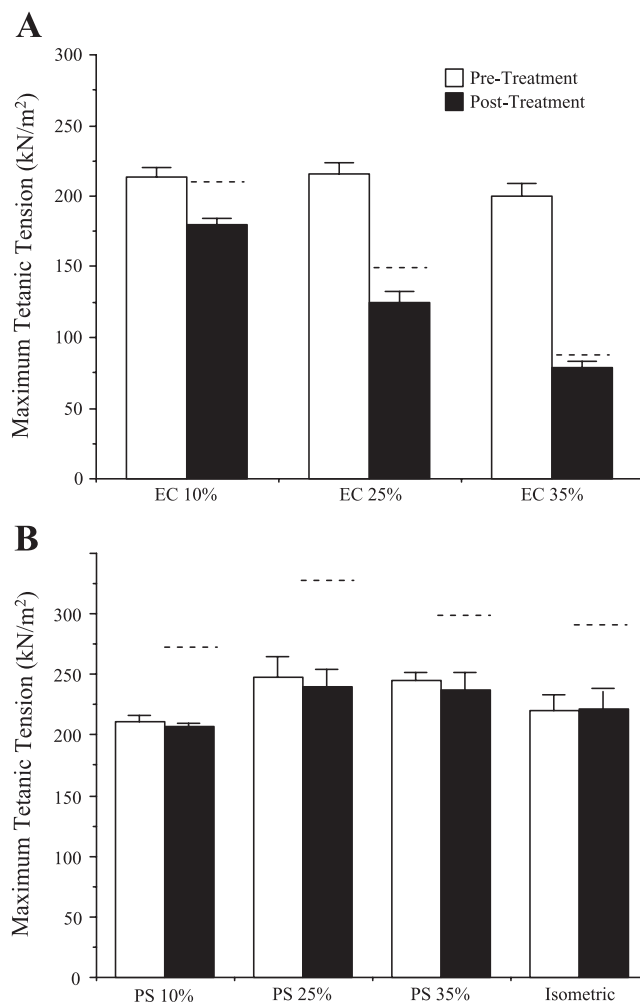


Fig. 4. Maximum tetanic tension (P_o) before (open bars) and 30 min after (solid bars) 10 EC of a nominal strain of 10, 25, or 35% (A) and 10 PS of a nominal strain of 10, 25, or 35% or isometric contraction (B). Values are means \pm SE. Dashed lines above solid bars represent mean of P_o 60 min after the addition of 10 mM caffeine to the bathing medium.

cantly below the potentiated stress resulting from caffeine application to passively stretched or isometrically activated uninjured muscles (Fig. 4B). Whereas a small increase was observed after incubation in Ringer + caffeine for the 25 and 35% groups, this increase was not nearly sufficient to reverse the P_o decline observed (Fig. 4A). It should be noted that others have demonstrated that nitrate, another calcium agonist, did not reverse the effects of EC on isolated frog muscle fibers (54).

No significant change was observed in P_o , measured before and after PS at any strain magnitude or after IC treatment ($P > 0.4$, Fig. 4B). As a positive control for the effects of caffeine treatment on frog skeletal muscle, the PS groups were incubated in Ringer + caffeine at the end of a series of 10 PS. These undamaged muscles demonstrated a significant 33% average increase in P_o relative to P_o without caffeine (Fig. 4B, dashed line above solid bars; $P < 0.05$).

Sarcomere strain and W during treatment. Passive sarcomere strain (ϵ_p) in each group subjected to PS remained constant across the 10-contraction treatment protocol (Fig. 2B, open symbols). Nominal fiber strains of 10, 25, and 35% resulted in actual measured values for ϵ_p of 0.09 ± 0.02 , 0.22 ± 0.013 , and 0.32 ± 0.03 , respectively, all of which were not significantly different from any of the target strains ($P > 0.2$), demonstrating the effectiveness of the method of fiber deformation application. Active sarcomere strain (ϵ_a) for each of the three groups subjected to EC also did not change significantly across the 10-contraction treatment protocol ($P > 0.6$; Fig. 3C). However, unlike ϵ_p , where fiber strain was equal to nominal strain, ϵ_a was more variable and was significantly less than the target strain for each of the three groups ($P < 0.001$). For the groups subjected to EC, ϵ_a was 0.085 ± 0.003 , 0.21 ± 0.008 , and 0.28 ± 0.005 for nominal fiber bundle strains of 10, 25, and 35%, respectively. This amounts to delivery of 85, 84, and 80% of the intended deformation to the sarcomere for the 10, 25, and 35% groups, respectively. Based on the measured properties of frog muscle series elastic element (28), as well as the frog tendon material properties (30, 38, 67), it is most likely that difference between measured and nominal strains resulted from a portion of the deformation taken up by the tendon. Still, the excellent correlation between imposed deformation and sarcomere strain validates that differential sarcomere strains were imposed on fiber bundles.

Given that direct measures of sarcomere strain were available, in contrast to previous studies in which sarcomere strain was assumed to be proportional to muscle deformation (37, 69), we used regression analysis to quantify the correlation between sarcomere strain and decline in muscle force. A significant relationship between sarcomere strain and percent decrease in P_o ($P < 0.0001$, $r^2 = 0.87$, Fig. 5) was observed, with the linear model accounting for ~87% of the experimental variability. No correlation was observed between peak stress and percent decrease in P_o ($P > 0.6$), although peak stress did not vary dramatically between groups and thus would not be expected to be a strong regressor.

W varied as expected for the IC and PS groups. These conditions are not novel and have been extensively studied previously (29, 34, 55, 56, 61, 62). A significant ~20% increase in W was observed with isometric activation as W increased from 893 ± 33 to $1,060 \pm 31$ pixels ($P < 0.001$), and a significant ~5% decrease in W from 897 ± 31 to 843 ± 29 pixels ($P < 0.05$) was measured at the end of PS. These

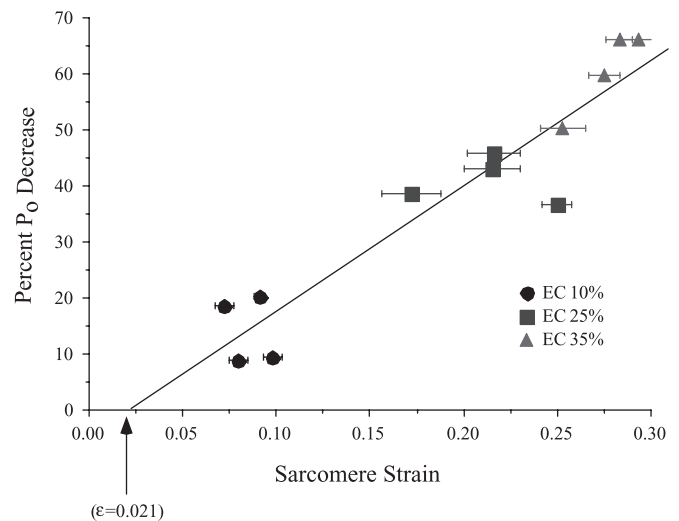


Fig. 5. Relationship between average sarcomere strain (ϵ) measured during the eccentric exercise bout and the loss in P_o measured 30 min after the exercise bout for each experimental group. Data are presented for 10% nominal eccentric strain (\bullet), 25% nominal eccentric strain (\blacksquare), and 35% nominal eccentric strain (\blacktriangle). A highly significant relationship between sarcomere strain and percent loss in P_o was observed ($P < 0.0001$). SE bars in strain direction represent the average variability measured across the 10 contractions for all muscles. Abscissa intercept at 0.021 (arrow) represents the theoretical sarcomere strain at which no injury would occur, determined by linear regression on the data points from each contraction.

results were consistent across the 10 IC and PS. The most interesting changes in W occurred with EC treatment. As expected, isometric activation caused an abrupt increase in W as force developed and sarcomeres shortened. Active stretch then resulted in a decrease in W (presumably due to the change in L_s as with PS), but the overall W value at the end of stretch increased with each subsequent stretch (Fig. 6). Samples from the 25 and 35% strain groups were pooled as they demonstrated yield points at essentially the same strain. For these samples ($n = 12$ total, 8–12 useable data points per contraction), the progressive increase in W was associated with a progressive decrease in yield force (Fig. 7), providing the intriguing possibility of a causal relationship between the two parameters. The same result was obtained for the pooled data compared with the results when the 25 and 35% groups were separated.

MHC percentages. Quantitative analysis of type 1 and type 2 MHC revealed no significant differences among the 10, 25, and 35% strain EC groups ($P > 0.4$) nor the 10, 25, and 35% strain PS groups ($P > 0.25$), with type 1 MHC percentage averaging $56 \pm 2.3\%$ ($n = 20$ specimens) across all specimens (Table 1). Thus the differential injury occurring across groups could not simply be explained by differences in fiber-type percentage among groups.

DISCUSSION

The purpose of this study was to elucidate the relationship between sarcomere behavior and muscle injury during ECs. This was accomplished by performing real-time measurement of laser diffraction patterns and fiber bundle stress during a series of 10 ECs. The study revealed that 1) muscle fiber bundles are more resistant to strain-induced injury compared with isolated single fibers, 2) sarcomere strain is a strong

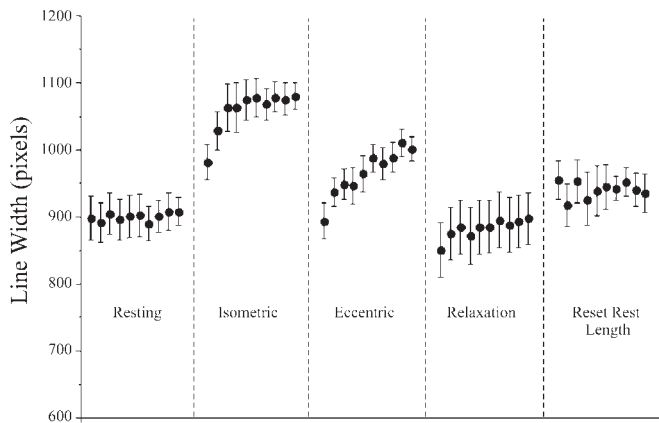


Fig. 6. Line width of first-order diffraction pattern measured at 5 different time periods of the EC shown in Fig. 1C and described in MATERIALS AND METHODS. Data are presented for (from left to right) the muscle at rest, after isometric activation, after active stretch ("active hold"), after relaxation ("passive hold"), and after return to resting length. The 10 symbols shown for each time period represent the 10 successive contractions imposed on the bundle. Values shown are means \pm SE.

predictor of the magnitude of muscle injury in small fiber bundles, and 3) injury is accompanied by a progressive increase in L_s heterogeneity and concomitant yield force decrease.

Comparison with previous studies of mechanical-based muscle injury. In two previous studies of mechanical factors affecting muscle injury, stress and strain were alternatively proposed as primary mechanical factors causing muscle injury (37, 69). The discrepancy between the studies may have been that comparison between the TA (37) and soleus muscles (69) was simply not valid due to the significant structural and functional differences between these muscles that have very different functions and very different fiber-type distributions. Indeed, in a study of EC-induced muscle injury to the rabbit soleus, we did find qualitatively different functional and struc-

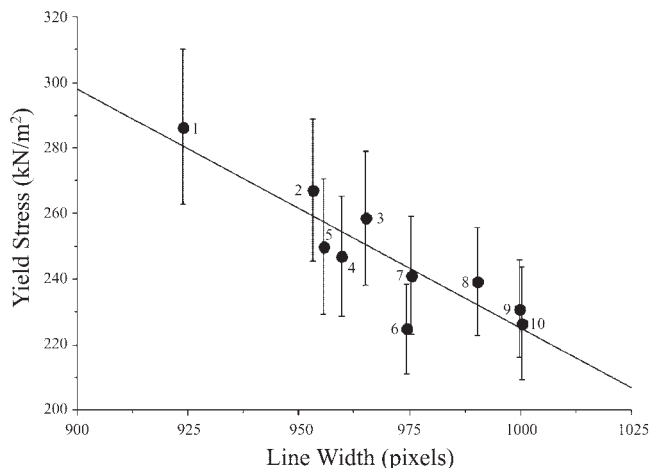


Fig. 7. Relationship between line width and yield stress for the 12 fiber bundles in the 25 and 35% strain EC groups. Values were expressed based on stress measurements to minimize variability due to differences in fiber number from each bundle. Numbers next to symbols are the contraction numbers (1–10) associated with each average value. Sample size ranges from 8 to 12 for each data point because useable diffraction patterns were not obtained for every contraction from every bundle. Values are means \pm SE.

Table 1. Myosin heavy chain content

Experimental Treatment Group	Type 1 MHC, %Total MHC Pool
Eccentric contraction	
10% Strain	57.4 \pm 6.7
25% Strain	61.4 \pm 3.4
35% Strain	56.7 \pm 5.1
Passive stretch	
10% Strain	54.6 \pm 2.1
25% Strain	48.1 \pm 7.1
35% Strain	48.9 \pm 6.6

Values are means \pm SE ($n = 4/\text{group}$) of type 1 myosin heavy chain (MHC) percentage. Because only types 1 and 2 MHC were present in these samples (43), type 2 MHC percentage = 100% value shown for each group.

tural effects of cyclic EC on soleus compared with TA muscle: rabbit soleus muscles showed no gross structural abnormalities; there was no evidence of cytoskeletal protein loss; and the magnitude of the force decline, even under extreme conditions, was much less than that observed for equivalent treatment of the TA (6). Thus it is possible that soleus muscles, perhaps due to the repetitive eccentric activation pattern that they normally experience, are simply more resistant to ECs and have developed different structures to resist injury that would be manifested after equivalent treatment of a muscle containing primarily fast fibers (39).

It is also possible that the conflicting data reported between rabbit TA and rat soleus muscles resulted from the different methods used to alter muscle stress. Whereas it is clear that both methods did, in fact, alter muscle stress, the actual strain imposed on the muscle fibers under the different conditions was not known. If one assumes that the altered stress conditions of both studies did not systematically bias sarcomere strain calculated, results of both studies could be valid and, indeed, conflicting. However, based on the nonlinear mechanical properties of the tendinous material in series with the muscle, identical deformation patterns applied to muscles contracting at different stresses could result in different sarcomere strains because deformation would be differentially distributed along the muscle and the compliant tendon. A final difference between the studies reported is that the range of the length-tension curve over which both muscles were stretched was not matched, and optimal length was not reestablished after injury using tetanic contractions. As mentioned above, a shift in muscle optimal length can lead to erroneous conclusions regarding the magnitude of injury. Clearly, all of these parameters must be measured directly if future studies are to be compared accurately. By using these arguments, serious questions could be raised regarding the actual sarcomere strain imposed in either of the previous studies. That uncertainty was eliminated here by use of direct L_s measurement. It was not possible to test the effects of altered stress explicitly in these experiments as, unexpectedly, peak stresses achieved among the three strain groups were not significantly different (Fig. 3A). This was surprising because isometric tension measured just before the EC varied significantly among the three groups (Fig. 3B).

A simple hypothesis for the dissociation between force generated (Fig. 3B) and force borne (Fig. 3A) by the contractile apparatus is that, during the EC protocol, cross bridges attach normally but yet do not enter the force-generating state. As the

cross-bridge mechanism is known to be a multistate phenomenon, this remains an intriguing possibility. It could even have functional significance in that muscles that experience significant injury are yet able to act as significant “brakes” during the eccentric action itself. It is also possible that the peak stress measured during EC is partly borne by structural elements that are not stressed during IC. Whether this is truly the case remains to be determined.

Excitation-contraction coupling and muscle injury. In a previous study, based on experiments on skinned muscle fibers, uncoupling of the excitation system from the contractile apparatus was hypothesized to cause almost all of the force decline observed after EC (68). To test the extent to which this could explain our contractile data, P_o was measured after the addition of 10 mM caffeine to the bathing medium. In muscles subjected to either PS or isometric activation and that demonstrated no signs of injury, P_o was potentiated by an average of $33.1 \pm 5.7\%$ (dotted lines, Fig. 4B). Using this as the nominal potentiation magnitude of caffeine, we compared the measured caffeine-potentiated P_o (dotted lines, Fig. 4A) to a P_o value 33% greater than the pre-EC value. A differential effect of caffeine on muscle force recovery was seen where 27, 14, and 4% of the force was recovered for the 10, 25, and 35% groups, respectively. This suggests that the magnitude of disruption of the excitation-contraction coupling apparatus was relatively small and strain dependent in this model. By far the majority of the loss in force was due to factors other than failure to release calcium from the sarcoplasmic reticulum. This is consistent with results from single-fiber studies in which the potentiator nitrate did increase calcium release (as measured by calcium binding dyes) but failed to reverse the change in optimal length induced by ECs (54).

Uniformity of applied deformation. To interpret the present data in terms of sarcomere strain without the confounding effects of intersarcomere dynamics, it was important that L_s measured near the fixed ends be representative of those occurring along the L_f . There is ample evidence from studies of isolated single frog muscle fibers that regional nonuniformities along the L_f can alter even the isometric tension generated by the fiber (1, 20, 27, 35). It has also been claimed that highly elongated sarcomeres occur in various regions along the isolated soleus fiber after EC (47). However, we do not believe that such regional differences in L_s occurred with our model. We claim that the L_s measured near the fixed bundle end were indeed representative (although not necessarily identical in magnitude) of changes that occurred along the entire fiber bundle length. This is because, despite the fact that shortening end sarcomeres and stretching central sarcomeres have been observed in isolated frog single fibers, there is no evidence that such L_s differences occur either at the whole muscle or fiber bundle level. If all “central” sarcomeres in the bundles used were forced to lengthen due to sarcomere shortening of “end” sarcomeres, average L_s , as indicated by laser diffraction, would have decreased during “fixed-end” activation. This was not the case for any of the fiber bundles studied. Of the 60 ICs measured from six different fiber bundles, after the initial sarcomere shortening occurred, subsequent L_s change to the end of the stimulation period was only $0.057 \pm .007 \mu\text{m}$ ($n = 60$), which was not significantly different from zero ($P > 0.3$). We also believe that the sarcomere strains during EC were representative of those sarcomere strains imposed along the

fiber bundle length. If regional nonuniformity of stretch during EC existed based on random intrinsic differences of sarcomere properties along and across the fiber bundles, some stretches could result in greater and others in lesser sarcomere strain along the L_f compared with the target strain. In fact, sarcomere strain as a function of EC number was fairly consistent throughout the treatment period (Fig. 3C) and always somewhat less than the target strain. If severe regional nonuniformities had developed along the L_f , sarcomere strain would occasionally be much larger than the nominal strain, as sarcomere populations were forced to absorb a disproportionate fraction of the length change. The fact that, in 180 ECs measured from 18 different fiber bundles at 3 different applied nominal strains, ϵ_a was always slightly less than the applied strain argues strongly against gross nonuniformities developing during the experiments. Clearly, most of the applied deformation was absorbed by the fiber region examined because 85% of the 10% strain, 84% of the 25% strain, and 80% of the 35% strain were delivered to the sarcomeres.

Experimental errors associated with laser diffraction. Although strain was applied to the sarcomere lattice in a fairly uniform manner, this does not preclude the possibility of the existence of a small population of sarcomeres within the illuminated region that could have rapidly elongated during EC but that would not be detected by laser diffraction. This idea was proposed to explain a number of unusual properties of actively lengthening skeletal muscle (52) and is supported experimentally (22, 46, 65, 71). Because laser diffraction yields average length of illuminated sarcomeres, weighted for uniformity, it is reasonable to expect that small populations of sarcomeres could remain “invisible” to the experimental method (34, 51). However, despite the possibility of “false negative” reporting using this technique, the opposite problem, “false positive” reporting of L_s , is not possible. Thus the sarcomere strains reported here do represent actual sarcomeres within the fiber bundle and are not artifacts of the diffraction method. If a population of invisible sarcomeres did rapidly elongate in a region outside of the illuminated region, the remaining sarcomeres in series would have shortened to compensate for the altered length or, at least, would not have elongated to the extent measured here. The quantitative L_s data argue that, in the region studied, invisible sarcomeres did not contribute substantially to the observed effect. We do not oppose the notion that sarcomeres within the illuminated region may have “popped” as proposed. Indeed, it would be expected, based on the theory (52) that a greater number of sarcomeres would experience undamped elongation as strain increased. This is because a greater number of sarcomeres would achieve the critical length necessary for undamped elongation (52).

It has been demonstrated that spurious L_s may be obtained by using laser diffraction on isolated single-muscle fibers, when the three-dimensional sarcomere lattice orientation satisfies the criterion of Bragg interference (59) or when subpopulations of sarcomeres diverge in lengths (34, 51). The magnitude of the Bragg effect was quantified in single fibers as a function of fiber size and beam diameter (41) and shown to be explainable by using a generalized three-dimensional light diffraction theory (5, 72). Such three-dimensional satisfaction of the Bragg condition across an entire fiber bundle is not possible because of the high degree of spatial and angular

A-band dispersion that occurs between muscle fibers. Pilot studies using fiber bundles of 15–50 fibers revealed intensity fluctuations of only ~15% compared with the 10-fold change obtained by using single fibers (data not shown). Using an average fiber bundle size of 60 fibers, a completely uniformly oriented fiber would contribute, at most, 1.7% of the intensity of a given diffraction order (1/60). More realistic measurements demonstrate that, under worst case conditions, ~15% of the diffraction order intensity from a single fiber can result from Bragg interference (41). We thus suspect that, at most, only ~0.3% of our diffraction pattern intensity (i.e., 15% of 1.7%) resulted from Bragg diffraction within muscle fiber bundles, which would not affect the L_s reported here.

The laser diffraction method provides the unique opportunity to define the L_s distribution within the illuminated region. Diffraction order W has been shown theoretically (34, 72) and experimentally (55, 56, 62) to estimate L_s variance within the illuminated region. In this experiment, significant increases in W were observed secondary to muscle activation (Fig. 6), supporting the concept proposed previously that muscle activation causes a redistribution of L_s in a random but not systematic fashion (see case III, Eq. 22 of Ref. 72). However, unexpectedly, W also progressively increased with each subsequent stretch (Fig. 6), and this W increase was accompanied by a systematic decrease in yield force (Fig. 7). This relationship was significant and linear in 14 of the 18 bundles tested, with correlation coefficients ranging from 0.61 to 0.93. Such an association between L_s heterogeneity and yield force was predicted as an ancillary feature of the “popping sarcomere” hypothesis (52) but has never been demonstrated experimentally. Morgan simulated the force records from hypothetical fibers in which heterogeneity ranged from 2% to 10% and showed precisely this yield force decrement. The functional explanation is that yield force reflects the weakest sarcomere being stretched. As heterogeneity increases, the weakest sarcomere becomes progressively weaker (and longer), thus resulting in a lower yield force. Whereas evidence for the existence of such “popped” sarcomeres was provided based on direct observation and statistical analysis of L_s from a fixed muscle (8, 65), this is the first direct demonstration of such a relationship in a population of living muscle fibers. It should be noted that, using a skinned rat soleus single-fiber model and attempting to measure L_s along the fiber, Macpherson and colleagues (47) claimed to provide direct experimental support for the popping sarcomere hypothesis. However, the “popped” sarcomeres that they reported (“longest” open bar in their Fig. 5) were only calculated by subtraction from actual experimental data and were never directly measured. This was because the authors could not obtain useable diffraction patterns in certain regions of the fiber after single ECs. This severely limits the interpretation of their data because it is not justified to assume that the entire deformation magnitude was taken up in the region for which no L_s was even measurable. Thus we claim that, using the EC model, there is presently no evidence for large-scale regional variation in L_s , as has been claimed (47), and, in fact, the present study provides data to counter that statement. It is most likely that the elongated sarcomeres are randomly distributed throughout the cell (52).

Sarcomere strain and muscle injury. Our data revealed that the magnitude of muscle injury, indicated by the decline in P_o , was a strong function of ϵ_a (Fig. 5). The relationship between

strain and percent tetanic tension decline was given by the equation y (% P_o decline) = 225 (% P_o decline/strain) \times strain – 4.78 ($P < 0.01$, $r^2 = 0.88$). Solving for the strain at which the % P_o decline is zero yields a value of 2.1%. Taken at face value, this suggests that, under the conditions used here, sarcomere strains of 2.1% would result in no muscle injury. This value is a reasonable approximation of the short-range elastic element in muscle corresponding to the high-stiffness portion of the eccentric curve (see, for example, the force record in Fig. 1C). The strain injury may only be initiated when muscle cross bridges are forcibly pulled off of the thin filament within the sarcomere and forced to reattach at a new active site closer to the specific cross bridge. In fact, injury could result from “overstraining” any element within the fiber. In the context of “sarcomere popping,” as mentioned above, greater strain would permit more sarcomeres to approach their “yield phase” and rapidly elongate, resulting in tissue injury.

Taken together, the present experiments provide strong support for the concept that mechanical injury to muscle is directly related to the sarcomere strain imposed on the sarcomere lattice. Furthermore, the progressive increase in L_s heterogeneity (Fig. 6) and the concomitant decrease in yield force (Fig. 7) provide strong support for the novel hypothesis of popping sarcomeres previously proposed.

ACKNOWLEDGMENTS

We thank Shannon Bremner for performing the SDS-PAGE processing and analysis and Michel Sam for performing the quantitative comparison of L_t measuring methods.

GRANTS

This work was supported by the Department of Veterans Affairs, National Institute of Arthritis and Musculoskeletal and Skin Diseases Grant AR-40050, the Swedish National Centre for Research in Sports, and the Lundberg Foundation.

REFERENCES

1. **Altringham JD and Bottinelli R.** The descending limb of the sarcomere length-force relation in single muscle fibers of the frog. *J Muscle Res Cell Motil* 6: 585–600, 1985.
2. **Bahler AS, Fales JT, and Zierler KL.** The dynamic properties of mammalian skeletal muscle. *J Gen Physiol* 51: 369–384, 1968.
3. **Balnavae CD and Allen DG.** Intracellular calcium and force in single mouse muscle fibres following repeated contractions with stretch. *J Physiol* 488: 25–36, 1995.
4. **Banes AJ.** Mechanical strain and the mammalian cell. In: *Physical Forces and the Mammalian Cell*, edited by Frangos JA. San Diego, CA: Academic, 1993, p. 81–123.
5. **Baskin RJ, Lieber RL, Oba T, and Yeh Y.** Intensity of light diffraction from striated muscle as a function of incident angle. *Biophys J* 36: 759–773, 1981.
6. **Benz RJ, Fridén J, and Lieber RL.** Simultaneous stiffness and force measurements reveal subtle injury to rabbit soleus muscles. *Mol Cell Biochem* 122: 312–319, 1998.
7. **Brooks SV, Zerba E, and Faulkner JA.** Injury to muscle fibres after single stretches of passive and maximally stimulated muscles in mice. *J Physiol* 488: 459–469, 1995.
8. **Brown LM and Hill L.** Some observations on variations in filament overlap in tetanized muscle fibres and fibres stretched during a tetanus, detected in the electron microscope after rapid fixation. *J Muscle Res Cell Motil* 12: 171–182, 1991.
9. **Burkholder TJ and Lieber RL.** Sarcomere length operating range of muscles during movement. *J Exp Biol* 204: 1529–1536, 2001.
10. **Cleworth DR and Edman K.** Changes in sarcomere length during isometric tension development in frog skeletal muscle. *J Physiol* 227: 1–17, 1972.

11. **Close RI.** The relations between sarcomere length and characteristics of isometric twitch contractions of frog sartorius muscle. *J Physiol* 220: 745–762, 1972.
12. **Edman K.** The relation between sarcomere length and active tension in isolated semitendinosus fibres of the frog. *J Physiol* 183: 407–417, 1966.
13. **Edman K, Mulieri LA, and Scubon MB.** Non-hyperbolic force-velocity relationship in single muscle fibres. *Acta Physiol Scand* 98: 143–156, 1976.
14. **Evans WJ, Meredith CN, Cannon JG, Dinarello CA, Frontera WR, Hughes VA, Jones BH, and Knuttgen HG.** Metabolic changes following eccentric exercise in trained and untrained men. *J Appl Physiol* 61: 1864–1868, 1986.
15. **Fridén J, Sjöström M, and Ekblom B.** A morphological study of delayed muscle soreness. *Experientia* 37: 506–507, 1981.
16. **Fridén J, Sjöström M, and Ekblom B.** Myofibrillar damage following intense eccentric exercise in man. *Int J Sports Med* 4: 170–176, 1983.
17. **Fujime S.** Optical diffraction study of muscle fibers. *Biochim Biophys Acta* 379: 227–238, 1975.
18. **Garrett WE Jr, Safran MR, Seaber AV, Glisson RR, and Ribbeck BM.** Biomechanical comparison of stimulated and nonstimulated skeletal muscle pulled to failure. *Am J Sports Med* 15: 448–454, 1987.
19. **Gordon AM, Huxley AF, and Julian FJ.** Tension development in highly stretched vertebrate muscle fibres. *J Physiol* 184: 143–169, 1966.
20. **Gordon AM, Huxley AF, and Julian FJ.** The variation in isometric tension with sarcomere length in vertebrate muscle fibres. *J Physiol* 184: 170–192, 1966.
21. **Guharay F and Sachs F.** Stretch-activated single ion channel currents in tissue-cultured embryonic chick skeletal muscle. *J Physiol* 352: 685–701, 1984.
22. **Harry JD, Ward AW, Heglund NC, Morgan DL, and McMahon TA.** Cross-bridge cycling theories cannot explain high-speed lengthening behavior in frog muscle. *Biophys J* 57: 201–208, 1990.
23. **Hill DK.** Tension due to interaction between the sliding filaments in resting striated muscle. The effect of stimulation. *J Physiol* 199: 637–684, 1968.
24. **Huxley AF.** Muscle structure and theories of contraction. *Prog Biophys Mol Biol* 7: 255–318, 1957.
25. **Ingber DE.** Fibronectin controls capillary endothelial cell growth by modulating cell shape. *Proc Natl Acad Sci USA* 87: 3579–3583, 1990.
26. **Julian FJ and Morgan DL.** The effect on tension of non-uniform distribution of length changes applied to frog muscle fibres. *J Physiol* 293: 379–392, 1979.
27. **Julian FJ and Morgan DL.** Intersarcomere dynamics during fixed end tetanic contractions of frog muscle fibers. *J Physiol* 293: 365–378, 1979.
28. **Katz B.** The relation between force and speed in muscular contraction. *J Physiol* 96: 45–64, 1939.
29. **Kawai M and Kunz ID.** Optical diffraction studies of muscle fibers. *Biophys J* 13: 857–876, 1973.
30. **Kawakami Y and Lieber RL.** Interaction between series compliance and sarcomere kinetics determines internal sarcomere shortening during fixed-end contraction. *J Biomech* 33: 1249–1255, 2000.
31. **Laemmli UK.** Cleavage of structural proteins during the assembly of the head of bacteriophage T4. *Nature* 227: 680–685, 1970.
32. **Lännergren J.** Contractile properties and myosin isoenzymes of various kinds of *Xenopus* twitch muscle fibres. *J Muscle Res Cell Motil* 8: 260–273, 1987.
33. **Lännergren J and Hoh JFY.** Myosin isozymes in single muscle fibers of *Xenopus laevis*: analysis of five different functional types. *Proc R Soc Lond B Biol Sci* 222: 401–408, 1984.
34. **Leung AF.** Calculation of the laser diffraction intensity of striated muscle by numerical methods. *Comput Programs Biomed* 15: 169–174, 1982.
35. **Lieber RL and Baskin RJ.** Intersarcomere dynamics of single muscle fibers during fixed-end tetani. *J Gen Physiol* 82: 347–364, 1983.
36. **Lieber RL and Fridén J.** Selective damage of fast glycolytic muscle fibers with eccentric contraction of the rabbit tibialis anterior. *Acta Physiol Scand* 133: 587–588, 1988.
37. **Lieber RL and Fridén J.** Muscle damage is not a function of muscle force but active muscle strain. *J Appl Physiol* 74: 520–526, 1993.
38. **Lieber RL, Leonard ME, Brown CG, and Trestik CL.** Frog semitendinosus tendon load-strain and stress-strain properties during passive loading. *Am J Physiol Cell Physiol* 261: C86–C92, 1991.
39. **Lieber RL, McKee-Woodburn T, and Fridén J.** Muscle damage induced by eccentric contractions of 25% strain. *J Appl Physiol* 70: 2498–2507, 1991.
40. **Lieber RL, Thornell LE, and Fridén J.** Muscle cytoskeletal disruption occurs within the first 15 minutes of cyclic eccentric contraction. *J Appl Physiol* 80: 278–284, 1996.
41. **Lieber RL, Yeh Y, and Baskin RJ.** Sarcomere length determination using laser diffraction. Effect of beam and fiber diameter. *Biophys J* 45: 1007–1016, 1984.
42. **Lutz GJ, Bremner SN, and Lieber RL.** Identification of myosin light chains in Rana pipiens skeletal muscle and their expression patterns along single fibers. *J Exp Biol* 204: 4237–4248, 2002.
43. **Lutz GJ, Cuizon DB, Ryan AF, and Lieber RL.** Four novel myosin heavy chain transcripts in Rana pipiens single muscle fibres define a molecular basis for muscle fibre types in the frog. *J Physiol* 508: 667–680, 1998.
44. **Lutz GJ, Sirsi SR, Shapard-Palmer SA, Bremner SN, and Lieber RL.** Influence of myosin isoforms on contractile properties of intact muscle fibers from Rana pipiens. *Am J Physiol Cell Physiol* 282: C835–C844, 2002.
45. **Lynch GS and Faulkner JA.** Contraction-induced injury to single muscle fibers: velocity of stretch does not influence the force deficit. *Am J Physiol Cell Physiol* 275: C1548–C1554, 1998.
46. **Lynn R and Morgan DL.** Decline running produces more sarcomeres in rat vastus intermedius muscle fibers than does incline running. *J Appl Physiol* 77: 1439–1444, 1994.
47. **Macpherson PC, Dennis RG, and Faulkner JA.** Sarcomere dynamics and contraction-induced injury to maximally activated single muscle fibres from soleus muscles of rats. *J Physiol* 500: 523–533, 1997.
48. **Marikhin VA and Myasnikova LP.** [Light diffraction by muscle fibers. I. Analysis of the geometric pattern of diffraction.] *Tsitologiya* 12: 1231–1236, 1970.
49. **McCully KK and Faulkner JA.** Injury to skeletal muscle fibers of mice following lengthening contractions. *J Appl Physiol* 59: 119–126, 1985.
50. **Mendez J and Keys A.** Density and composition of mammalian muscle. *Metabolism* 9: 184–188, 1960.
51. **Morgan DL.** Predictions of some effects on light diffraction patterns of muscles produced by areas with different sarcomere lengths (Abstract). *Biophys J* 21: 88a, 1978.
52. **Morgan DL.** New insights into the behavior of muscle during active lengthening. *Biophys J* 57: 209–221, 1990.
53. **Morgan DL and Allen DG.** Early events in stretch-induced muscle damage. *J Appl Physiol* 87: 2007–2015, 1999.
54. **Morgan DL, Claffin DR, and Julian FJ.** The effects of repeated active stretches on tension generation and myoplasmic calcium in frog single muscle fibres. *J Physiol* 497: 665–674, 1996.
55. **Oba T, Baskin RJ, and Lieber RL.** Light diffraction studies of active muscles fibres as a function of sarcomere length. *J Muscle Res Cell Motil* 2: 215–224, 1981.
56. **Paolini PJ and Roos KP.** Length-dependent optical diffraction pattern changes in frog sartorius muscle. *Physiol Chem Phys* 7: 235–254, 1975.
57. **Paolini PJ, Roos KP, and Baskin RJ.** Light diffraction studies of sarcomere dynamics in single skeletal muscle fibers. *Biophys J* 20: 221–232, 1977.
58. **Proske U and Morgan DL.** Muscle damage from eccentric exercise: mechanism, mechanical signs, adaptation and clinical applications. *J Physiol* 537: 333–345, 2001.
59. **Rüdel R and Zite-Ferencyz F.** Interpretation of light diffraction by cross-striated muscle as Bragg reflexion of light by the lattice of contractile proteins. *J Physiol* 290: 317–330, 1979.
60. **Sam M, Shah S, Fridén J, Milner DJ, Capetanaki Y, and Lieber RL.** Desmin knockout muscles generate lower stress and are less vulnerable to injury compared to wild-type muscles. *Am J Physiol Cell Physiol* 279: C1116–C1122, 2000.
61. **Sadow A.** Diffraction patterns of the frog sartorius and sarcomere behavior during contraction. *J Cell Comp Physiol* 9: 55–75, 1936.
62. **Sadow A.** Diffraction patterns of the frog sartorius and sarcomere behavior under stretch. *J Cell Comp Physiol* 9: 37–54, 1936.
63. **Sokal RR and Rohlf FJ.** *Biometry*. San Francisco, CA: Freeman, 1981.
64. **Stauber WT, Fritz VK, Vogelbach DW, and Dahlmann B.** Characterization of muscles injured by forced lengthening. I. Cellular infiltrates. *Med Sci Sports Exerc* 20: 345–353, 1988.

65. **Talbot JA and Morgan DL.** Quantitative analysis of sarcomere non-uniformities in active muscle following a stretch. *J Muscle Res Cell Motil* 17: 261–268, 1996.
66. **Talmadge RJ and Roy RR.** Electrophoretic separation of rat skeletal muscle myosin heavy-chain isoforms. *J Appl Physiol* 75: 2337–2340, 1993.
67. **Trestik CL and Lieber RL.** Relationship between achilles tendon mechanical properties and gastrocnemius muscle function. *J Biomech Eng* 115: 225–230, 1993.
68. **Warren GL, Lowe DA, Hayes DA, Karwoski CJ, Prior BM, and Armstrong RB.** Excitation failure in eccentric contraction-induced injury of mouse soleus muscle. *J Physiol* 468: 487–499, 1993.
69. **Warren GW, Hayes D, Lowe DA, and Armstrong RB.** Mechanical factors in the initiation of eccentric contraction-induced injury in rat soleus muscle. *J Physiol* 464: 457–475, 1993.
70. **Whitehead NP, Allen TJ, Morgan DL, and Proske U.** Damage to human muscle from eccentric exercise after training with concentric exercise. *J Physiol* 512: 615–620, 1998.
71. **Wood SA, Morgan DL, and Proske U.** Effects of repeated eccentric contractions on structure and mechanical properties of toad sartorius muscle. *Am J Physiol Cell Physiol* 265: C792–C800, 1993.
72. **Yeh Y, Baskin RJ, Lieber RL, and Roos KP.** Theory of light diffraction by single skeletal muscle fibers. *Biophys J* 29: 509–522, 1980.

